Ab initio study on the lattice instability of silicon and aluminum under [0 0 1] tension

Yashiro, Kisaragi

Oho, Masashi

Tomita, Yoshihiro

Ab initio study on the lattice instability of silicon and aluminum under [001] tension

Kisaragi Yashiro [a,*] Masashi Oho [b] Yoshihiro Tomita [c]

[a] *Department of Mechanical Engineering, Faculty of Engineering, Kobe University, Rokkodai, Nada, Kobe 657-8501, Japan*

[b] *Sumitomo Electric Industries, Co. LTD.*

[c] *Graduate School of Science and Technology, Kobe University, Rokkodai, Nada, Kobe 657-8501, Japan*

Abstract

Two different single crystals, Si with the diamond structure and Al with face-centered-cubic, are subjected to [001] tension in *ab initio* molecular dynamics (static) simulations based on BHS pseudopotential. Not only the ideal tensile strength under isotropic Poisson contraction, but also the crystal stability and bifurcation to anisotropic contraction are discussed in terms of the elastic stiffness matrix and the change in the charge density. The ideal tensile strengths are overestimated to as high as $\varepsilon = 0.18,\ \sigma = 18.7\,\mathrm{GPa}$ for Si and $\varepsilon = 0.25,\ \sigma = 23.5\,\mathrm{GPa}$ for Al, respectively. These values are inconsistent with the experimentally observed characteristics such as the hardness of Al being lower than that of Si. The elastic stiffness matrix reveals that the crystals become unstable at far lower strain and stress, $\varepsilon = 0.094,\ \sigma = 10.7\,\mathrm{GPa}$ for Si and $\varepsilon = 0.055,\ \sigma = 5.65\,\mathrm{GPa}$ for Al, and bifurcate to the lower energy pass of the anisotropic contraction. The change in the electronic structure suggests that nucleation/passage of a partial dislocation would take place

in the bifurcated anisotropic contraction. Thus the instability point indicates the onset of the nonelastic deformation and is much more important than the ideal tensile strength.

Key words: Lattice Instability, *Ab initio* Molecular Dynamics, Bifurcation Criteria, Ideal Strength, Elastic Stiffness Coefficient, Silicon, Aluminum

1 Introduction

Ab initio simulation based on the density functional theory have great potential in material design since it can be used to precisely predict the actual structure and motion of atoms without any experimental data. The recent rapid progress in computers has made it possible to implement *ab initio* calculations of the mechanical properties as well as the static atomic structure. Sób et al. [1] studied the anisotropy of the tensile strength of tungsten and NiAl. Kohyama [2] carried out tensile simulations of SiC bicrystals and reported the ideal strength of the SiC grain boundary. Ogata and Kitagawa [3] also conducted *ab initio* tensile testing on Al, AlN and their composite. Umeno and Kitamura [4] and our research group [5] separately evaluated the shear strength of Si single crystals for a critical shear strain, with respect to dislocation nucleation. These *ab initio* simulations on deformation and fracture, however, are implemented with no more than a hundred atoms because of

* Corresponding author. Department of Mechanical Engineering, Faculty of Engineering, Kobe University, 1-1, Rokkodai-cho, Nada, Kobe 657-8501, Japan. Tel.:+81-78-803-6303; fax:+81-78-803-6155.
Email address: yashiro@mech.kobe-u.ac.jp (Kisaragi Yashiro).
URL: http://solid.mech.kobe-u.ac.jp/ (Kisaragi Yashiro).

computational limitation, so the ideal strength should be evaluated under the assumption that crystals deform in a definite deformation pass. That is, the crystals *cannot* change to another deformation pass even if they become unstable in the given pass, due to the deformation constraint arising as a result of the insufficient number of atoms. Thus it is important, in *ab initio* deformation analysis, to clarify the relationship between the ideal strength and the bifurcation to another deformation pass from the viewpoint of crystal instability.

The lattice instability analysis [6–8] based on the classical interatomic potentials, which was actively discussed in the 1970s, has revealed that the bifurcation to the anisotropic Poisson contraction may become more important than the ideal tensile strength in the case of uniaxial [001] tension. In fact, our molecular dynamics simulation of a nickel single crystal, which was based on the semi-empirical interatomic potential and involved a sufficient number of atoms, showed that the onset of anisotropic Poisson contraction brings about precursory deformation localization on the crystal and a dislocation nucleates there [9]. Thus the lattice instability analysis, which is basically limited to the ideal deformation of a homogeneous crystal, provides substantial insight on the deformation mechanism and criteria for a larger system. The *ab initio* calculation is well suited to lattice instabilty analysis since it cannot treat a large number of atoms but evaluates the system energy precisely. The formulation of stability criteria was also generalized by Wang and coworkers [10,11] from Born's conventional analytical method [12] to the computational method based on the elastic stiffness coefficients [13], which can be numerically calculated in the *ab initio* simulation.

In the present study, *ab initio* molecular dynamics (static) simulations are

conducted on single crystals of silicon and aluminum under [001] tension. The stress–strain curves and the ideal strengths are investigated under isotropic Poisson contraction. The crystal stability is also quantitatively evaluated at each strain in terms of the determinant of the elastic stiffness coefficients. The bifurcation to anisotropic contraction and the internal change in the electronic structure at the unstable point are also discussed.

2 Instability criteria based on elastic stiffness coefficients

The stress, σ_{ij}, and the elastic coefficient, C_{ijkl}, are defined as [13]

$$\sigma_{ij} = \frac{1}{V}\left(\frac{\partial U}{\partial \eta_{ij}}\right) \tag{1}$$

$$C_{ijkl} = \frac{1}{V}\left(\frac{\partial^2 U}{\partial \eta_{ij}\eta_{kl}}\right) \tag{2}$$

for the adiabatic process. Here, U is the internal energy, V the volume of the crystal and η_{ij} the virtual infinitesimal strain measured in the equilibrium state considered. Helmholtz's free energy F is substituted for U in the isothermal process. The elastic stiffness coefficient, B_{ijkl}, relates the stress described by Eq. (1) with the actual large strain, ε_{ij}, measured from the unloaded reference state via the following equation [13]:

$$\begin{aligned} B_{ijkl} &= \left(\frac{\partial \sigma_{ij}}{\partial \varepsilon_{kl}}\right) \\ &= C_{ijkl} + \frac{1}{2}(\sigma_{il}\delta_{jk} + \sigma_{jl}\delta_{ik} + \sigma_{ik}\delta_{jl} + \sigma_{jk}\delta_{il} - 2\sigma_{ij}\delta_{kl}), \end{aligned} \tag{3}$$

where δ_{ij} is Kronecker's delta. That is, the elastic stiffness coefficients represent the gradient of the nonlinear stress–strain curve. A crystal becomes unstable when the symmetric tensor of $B^{\mathrm{sym}}_{ijkl} = (B_{ijkl} + B_{lkji})/2$ loses its positiveness [10,11]. Taking account of the Voigt symmetry, the stability limit is

evaluated by the determinant of the 6×6 matrix of B_{IJ}, where B_{IJ} is the Voigt notation of B^{sym}_{ijkl}. In the case of [001] tension under isotropic Poisson contraction, nonzero components of B_{IJ} decrease to 6 independent parameters, $B_{11}, B_{12}, B_{13}, B_{33}, B_{44}$ and B_{66}, where $I = 3$ indicates the tensile direction.

3 Simulation procedure

Simulations are implemented using our *ab initio* molecular dynamics code of the pseudopotential plane wave (PP-PW) method based on the density functional theory (DFT) and local density approximation (LDA). The pseudopotential adopted is the normconserving *ab initio* pseudopotential of Bachelet–Hammann–Schlüter (BHS) [14]. The simulation for a Si single crystal is conducted using the supercell containing 8 atoms, shown in Fig. 1 (a). The k-points of $2\times2\times2$ are sampled in the Brillouin zone according to the Monkhorst-Pack scheme [15] and the cutoff energy is set to $E_{\mathrm{cut}} = 16.0$ Ry in the simulation for Si. On the other hand, the supercell with 4 atoms, shown in Fig. 1 (b), k-meshes of $3 \times 3 \times 3$ and $E_{\mathrm{cut}} = 20.0$ Ry are used in the simulation for the Al single crystal. The conditions are listed in Table 1. The cutoff energies and k-meshes are basically defined from the energy convergence tests. The number of k-meshes for Al, however, is the maximum of our calculation. It would be desirable to sample more k-points, however, the value is justified from another calculation of $13 \times 13 \times 13$ k-points using VASP (Vienna ab-initio simulation program) [16–18] with ultrasoft pseudopotential [19]. The equilibrium lattice constant is evaluated to be 0.5374 nm for Si and 0.3970 nm for Al, respectively, from the minimum energy of the supercells. Both values are about 1∼2% smaller than the experimental values of 0.5429 nm and

0.405 nm, respectively. This difference is expected for the *ab initio* calculation based on the DFT–LDA [20], and our calculations have sufficient precision in comparison with other *ab initio* results [3,4].

The strain increment of $\Delta\varepsilon_{zz} = 0.005$ or $\Delta\varepsilon_{zz} = 0.001$ is applied to the supercells along the z axis and the atomic structure is relaxed by means of *ab initio* molecular dynamics (static). Here, the lateral strain of ε_{xx} $(= \varepsilon_{yy})$ is varied with the interval of 0.0005 to make the transverse stresses of σ_{xx} and σ_{yy} zero. The sress is calculated with the *ab initio* formulation of Nielsen and Martin [21]. After finding the suitable lateral strain and atomic structure, the strain components are perturbed with the magnitude of ± 0.0005, as schematically illustrated in Fig. 2, in order to evaluate the elastic coefficients numerically from the change in the stress. Then the crystal stability is investigated using the stress and elastic coefficents. This procedure is repeated until the stress–strain curve reaches its peak, or the ideal tensile strength, under isotropic Poisson contraction.

4 Results and discussion

4.1 Ideal tensile strength and instability point

The changes in the system energy and the stress are shown in Figs. 3 and 4, respectively. Here, not the total energy but the free energy is indicated for Al in view of the noninteger occupation number near the Fermi level of the metallic system. The stress–strain behavior of both the Si and the Al single crystal is elastic since the simulations are conducted with homogeneous deformation of the unit lattice, although internal relaxation is permitted. The

curves, however, differ due to the lattice structure and the relaxation of internal strain in Si. The peak stresses are 18.7 GPa at $\varepsilon_{zz} = 0.25$ for Si and 23.5 GPa at $\varepsilon_{zz} = 0.18$ for Al, respectively. Thus the ideal strength indicates that silicon is weaker than aluminum in terms of the proof stress; however, this is clearly inconsistent with the experimental results.

The changes in the magnitude of the 6×6 determinant of B_{IJ}, which represents the crystal stability, are shown Fig. 5. The figure focuses on the change in the vicinity of the strain where the determinant changes its sign. Si loses its stability at $\varepsilon_{zz} = 0.094$ while Al does at $\varepsilon_{zz} = 0.052$, and the corresponding stresses are evaluated at $\sigma_{zz} = 10.7$ GPa and $\sigma_{zz} = 5.65$ GPa, respectively. From the viewpoint of crystal stability silicon has higher proof stress than aluminum; this coincides with the actual strengths, in contrast to the ideal tensile strength described above. Table 2 lists all nonzero components of B_{IJ} before and after the instability point. It is noteworthy that B_{11} becomes smaller than B_{12} at the critical strain. This makes the minor determinant of $B_{11}^2 - B_{12}^2$ negative and leads to the unstable condition of $\det B_{IJ} < 0$. This instability causes symmetry breaking in the lateral direction, or the crystals will bifurcate to the anisotropic Poisson contraction.

4.2 Bifurcation to the anisotropic Poisson contraction

In order to follow up the bifurcated deformation after the instability, the aspect ratio of the cell length in the lateral direction, L_y/L_x, is changed at the interval of 0.001 under the condition of constant volume. Figure 6 shows the change in the total energy of Si against the anisotropic contraction. The dashed line indicates the energy of the isotropic contraction, or the value at $L_x/L_y =$

1. It is clear that the isotropic contraction is the lowest energy pass before the instability strain of $\varepsilon_{zz} = 0.094$, as shown in Fig. 6 (a). The minimum point, however, shifts toward higher aspect ratio as the tensile strain increases beyond $\varepsilon_{zz} = 0.094$. The crystal will deform along the lowest energy pass of anisotropic contraction bifurcated from the instability strain of $\varepsilon_{zz} = 0.094$. Similar bifurcation can be seen in the free energy of Al, as shown in Fig. 7. The energy minumium shifts about 15% from the isotropic contraction at the strain of $\varepsilon_{zz} = 0.052$, where the crystal becomes unstable. The aspect ratio becomes much larger than that of Si, so the Al structure may change drastically from the bifurcation point.

Figure 8 illustrates the distributions of charge density on the (110) and $(\bar{1}10)$ planes of Si at the strain of $\varepsilon_{zz} = 0.099$, under the isotropic and the bifurcated anisotropic contraction. The inner core electrons are omitted in the pseudopotential, thus the charge density rapidly vanishes near the nuclei. In the isotropic contraction, the internal strain is relaxed to maintain the symmetric charge density. All bond charges of A∼D in the figure have the same intensity. On the other hand, the bond charge loses symmetry and increases at B and D bonds and decreases at A and C bonds in the anisotropic contraction. The bond change is schematically illustrated in Fig. 9. The thick line indicates the tightened bond, or the bonds shrinking back after stretching, while the wavy line indicates the weakened bond, or one that will elongate further. These bond changes lead to the atom migration indicated by the arrow in the figure, which corresponds to that induced by the nucleation/passage of a partial dislocation on the (111) slip plane.

The distributions of charge density of Al are shown in Fig. 10 for each of the isotropic and the bifurcated anisotropic contraction at $\varepsilon_{zz} = 0.052$. The figure

shows the distribution on the (111), ($1\bar{1}1$) and ($11\bar{1}$) planes. The distance between the nearest neighbors shrinks on the (001) plane due to lateral strain, while it expands on the (100) and (010) planes under [001] tension. Thus the charge density becomes higher at Point A on (001) than at Points B and C on (010) and (100) planes, as marked in Fig. 10 (a). The distribution is symmetric with respect to Points B and C, and the charge density on the (111), ($1\bar{1}1$) and ($11\bar{1}$) planes are the same in the isotropic contraction of Fig. 10 (a). In the case of the anisotropic contraction of Fig. 10 (b), the valence electrons between nearest neigbors decrease on the (100) plane while they increase on the (010) plane. There is no notable change in the density of nearest neighbors on the (001) plane. The change in the distribution of charge density is summarized in the schematic of Fig. 11. The thick line corresponds to the nearest neighbor where the charge density increases, while the wavy line is for the decreased one. The thick white line corresponds to the unchanged high valance density between atoms on the (001) plane. The elongated atom distance will shrink back for the thick line and expand further for the wavy one. By this change, Atom C will migrate toward the direction of the arrow in the figure, along the trigonal lattice of Atom A. This atom migration and other equivalent ones give rise to nucleation/glide of a partial dislocation.

5 Summary

Ab initio molecular dynamics (static) simulations were conducted on single crystals of Si with a diamond structure and Al with a face-centered-cubic lattice, respectively, under the [001] tension. Not only the ideal tensile strength under the isotropic Poisson contraction, but also the crystal stability and

bifurcation to the anisotropic contraction were discussed from the viewpoint of the elastic stiffness matrix and change in the charge density. The results are summarized as follows.

(1) The ideal tensile strengths were evaluated at $\varepsilon_{zz} = 0.18,\ \sigma_{zz} = 18.7\,\mathrm{GPa}$ for Si and $\varepsilon_{zz} = 0.25,\ \sigma_{zz} = 23.5\,\mathrm{GPa}$ for Al under isotropic Poisson contraction. These ideal strengths contradict the magnitude relationships of the experimentally observed characteristics, such as the hardness of Si and Al.

(2) The crystal stability was investigated by calculating the elastic stiffness matrix at each strain under tension. The determinant of the matrix becomes negative, i.e., the crystal became unstable, at $\varepsilon_{zz} = 0.094$ for Si and $\varepsilon_{zz} = 0.055$ for Al. The corresponding stresses were evaluated at $\sigma_{zz} = 10.7\,\mathrm{GPa}$ and $\sigma_{zz} = 5.65\,\mathrm{GPa}$, respectively.

(3) The minor determinant of $B_{11}^2 - B_{12}^2$, which is related to the symmetry in the lateral direction, became negative in both Si and Al at the instability point. This suggests that the crystals bifurcate to the anisotropic contraction from that point.

(4) *Ab inito* calculations on the anisotropic contraction revealed that the lowest energy pass actually bifurcates from the instabilty point. Detailed investigation on the change in charge density indicated that the atom migration, which is equivalent to that due to the nucleation/passage of a partial dislocation, would occur in the bifurcated deformation.

References

[1] M. Sób, L. G. Wang and V. Vitek, Phil. Mag. B, 78 (1998), 653–658.

[2] M. Kohyama, Phil. Mag. Lett., 79 (1999), 659–672.

[3] S. Ogata and H. Kitagawa, Comp. Mater. Sci., 15 (1999), 435–440.

[4] Y. Umeno and T. Kitamura, Mater. Sci. and Eng., B88 (2002), 79–84.

[5] Y. Kusunoki, Master thesis of Kobe University (2000).

[6] F. Milstein, Phys. Rev. B, 3 (1971), 1130–1141.

[7] R. Hill, Mathematical Proceedings of the Cambridge Philosopical Society, 77 (1975), 225–240.

[8] J. M. T. Thompson and P. A. Shorrock, J. Mech. Phys. Solids, 23 (1975), 21–37.

[9] K. Yashiro and Y. Tomita, Journal de Physique IV, 11 (2001), Pr5-3–Pr5-10.

[10] J. Wang, S. Yip, S. R. Phillpot and D. Wolf, Phys. Rev. Lett., 71 (1993), 4182–4185.

[11] J. Wang, J. Li, S. Yip, S. R. Phillpot and D. Wolf, Phys. Rev. B, 52 (1995), 12627–12635.

[12] M. Born and K. Huang, *Dynamical Theory of Crystal Lattices*, (1954), Oxford UP.

[13] D. C. Wallace, *Thermodynamics of Crystals*, (1972), Wiley, New York.

[14] G. B. Bachelet, D. R. Hamann and M. Schluter, Phys. Rev. B, 26 (1982), 4199–4228.

[15] H. J. Monkhorst and J. D. Pack, Phys. Rev. B, 13 (1976), 5188–5192.

[16] G. Kresse and J. Hafner, Phys. Rev. B, 47 (1993), 558–561; ibid. 49 (1994), 14251–14269.

[17] G. Kresse and J. Furthmüller, Comput. Mat. Sci., 6 (1996), 15–50.

[18] G. Kresse and J. Furthmüller, Phys. Rev. B, 54 (1996), 11169–11186.

[19] G. Kresse and J. Hafner, J. Phys.: Condens. Matt., (1994), 8245–8257.

[20] D. M. Ceperley and B. J. Alder, Phys. Rev. Lett., 45 (1980), 566–569.

[21] O. H. Nielsen and R. M. Martin, Phys. Rev. Lett., 50 (1983), 697–700.

captions.

Fig. 1.

Supercells of the unit lattices of Si and Al.

Fig. 2.

Schematic of the evaluation of elastic coefficients.

Fig. 3.

Relationship between total (or free) energy and applied strain.

Fig. 4.

Relationships between stress and applied strain.

Fig. 5.

Change in crystal stability under [001] tension with isotropic Poisson contraction.

Fig. 6.

Change in total energy under anisotropic contraction (Si).

Fig. 7.

Change in total energy under anisotropic contraction (Al).

Fig. 8.

Distribution of charge density on the (110) and ($\bar{1}$10) planes of Si under isotropic and bifurcated anisotropic contractions.

Fig. 9.

Schematic of change in bond charge of Si.

Fig. 10.

Distribution of charge density on the (111), ($1\bar{1}1$) and ($11\bar{1}$) planes of Al under isotropic and bifurcated anisotropic contractions.

Fig. 11.

Schematic of change in valence electron density between the nearest neighbors of Al.

Table 1

Conditions of *ab initio* calculation.

Material	Si	Al
Number of atoms	8	4
Lattice constant (in nm)	0.5374	0.3970
Cutoff energy (in Ry)	16.0	20.0
k-mesh	$2 \times 2 \times 2$	$3 \times 3 \times 3$
Pseudopotential	BHS	BHS

Table 2

Components of the elastic stiffness coefficients calculated at the strain before and after the instability point.

	ε_{zz}	B_{11}	B_{12}	B_{33}	B_{13}	B_{44}	B_{66}
Si	0.093	196.4	195.2	234.3	162.2	29.5	39.8
	0.094	195.2	197.5	231.8	153.2	28.9	39.6
Al	0.051	225.6	224.3	242.2	111.4	42.2	31.6
	0.052	225.4	225.5	242.2	109.0	42.2	31.3

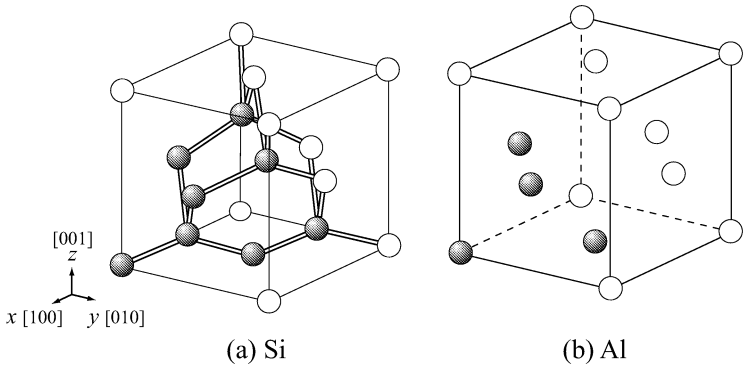

Fig. 1.

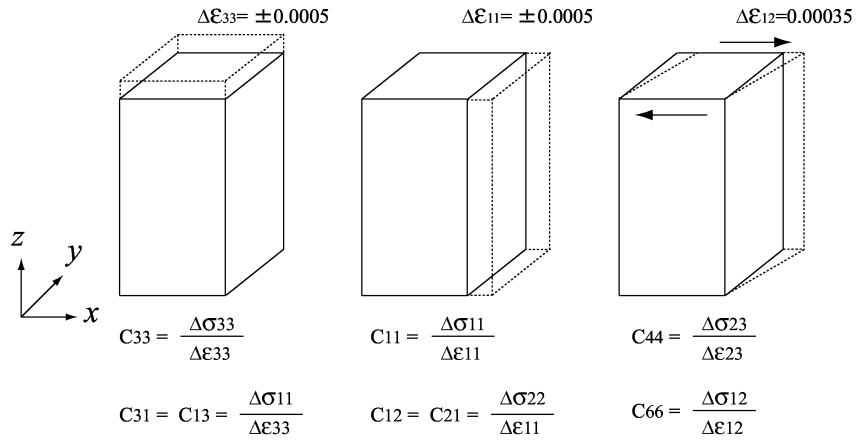

Fig. 2.

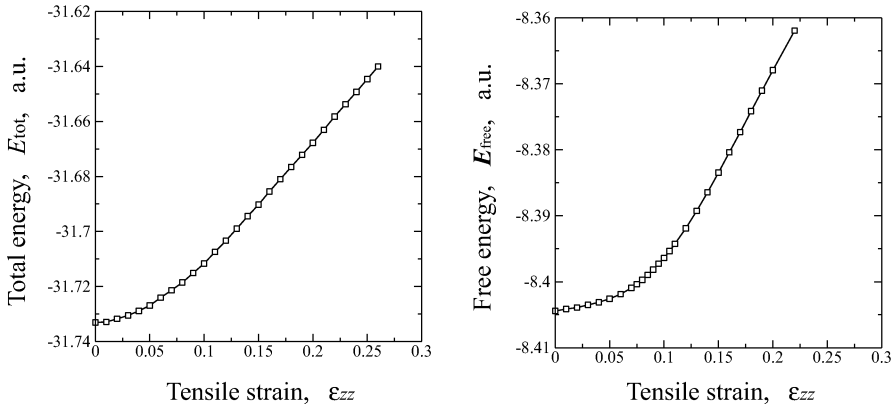

(a) Si (b) Al

Fig. 3.

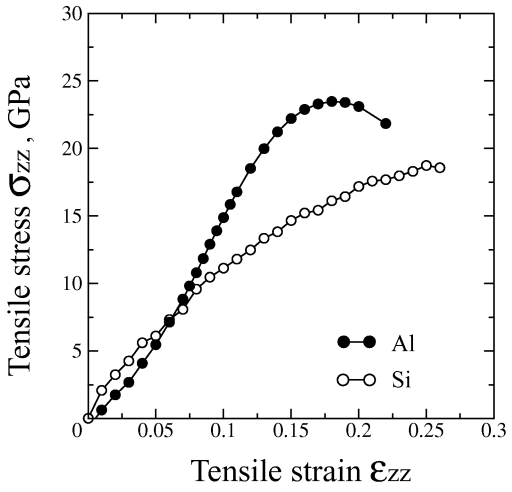

Fig. 4.

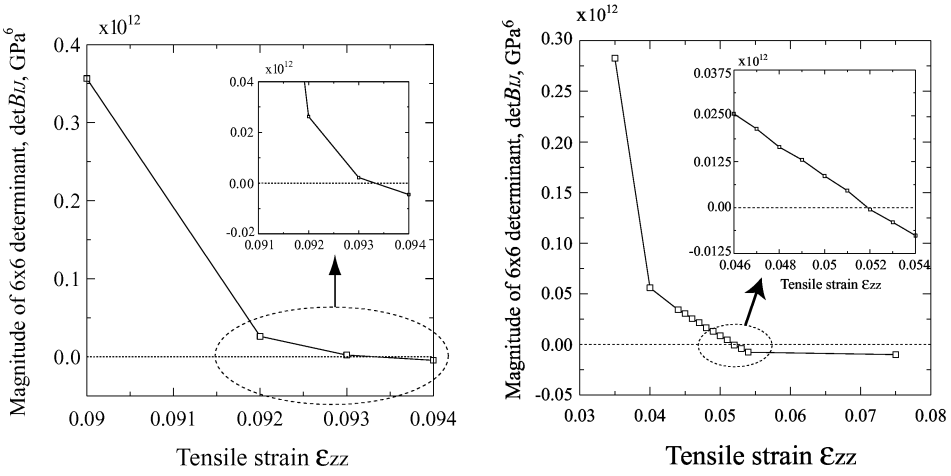

(a) Si (b) Al

Fig. 5.

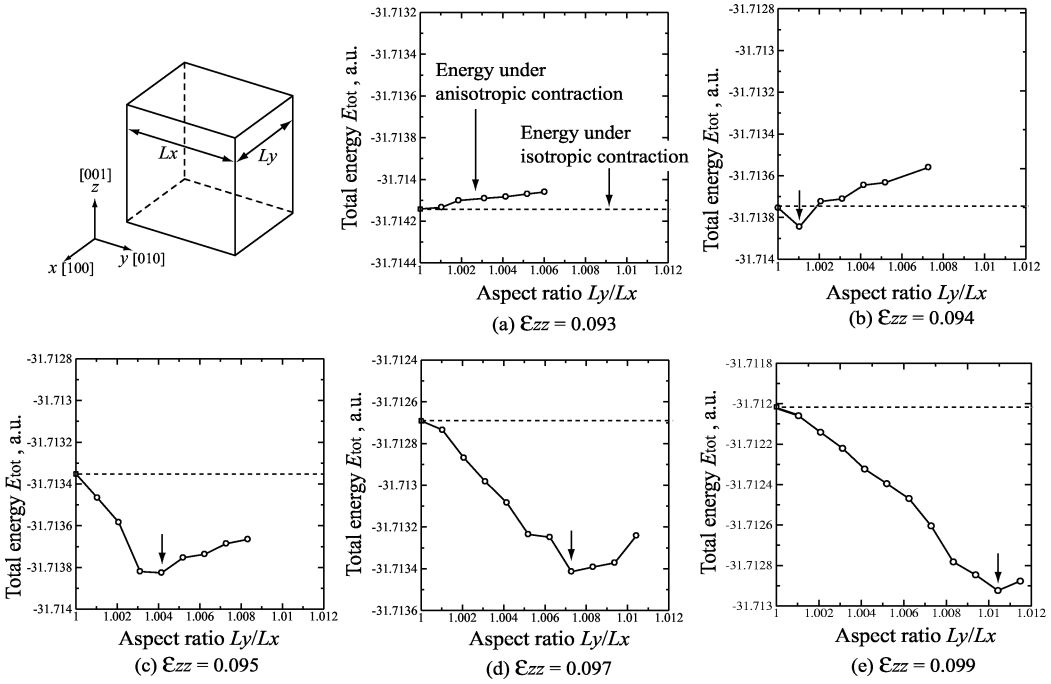
Lx
Ly
[001]
z
x [100]
y [010]
Energy under
anisotropic contraction
Energy under
isotropic contraction
Total energy Etot , a.u.
Aspect ratio Ly/Lx
(a) εzz = 0.093
(b) εzz = 0.094
(c) εzz = 0.095
(d) εzz = 0.097
(e) εzz = 0.099

Fig. 6.

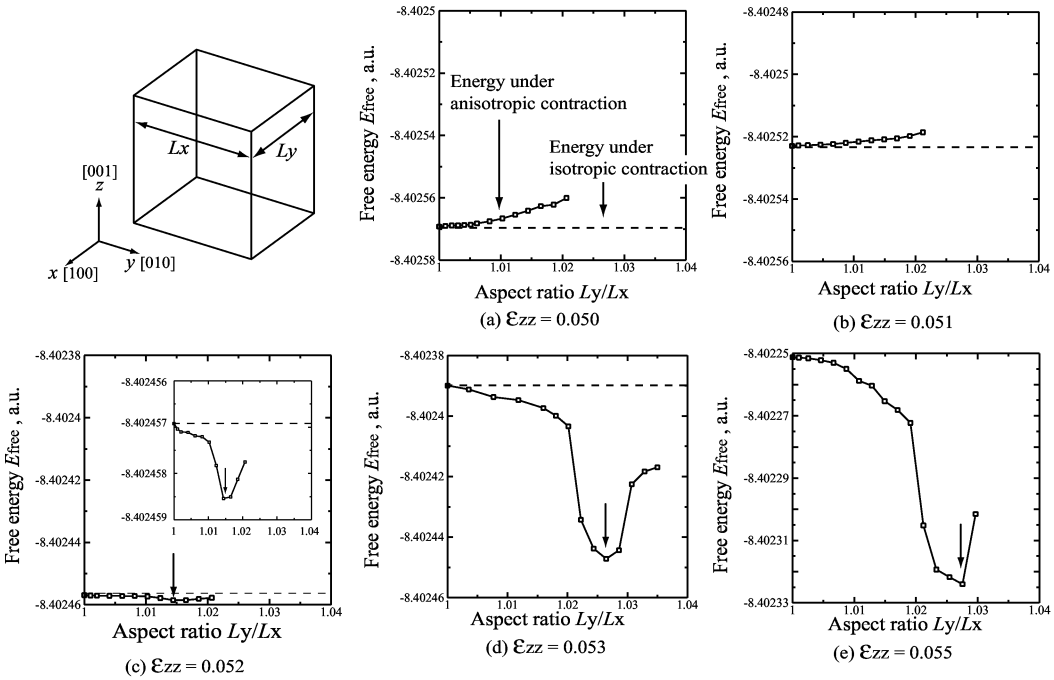
Lx
Ly
[001]
z
x [100]
y [010]
Energy under
anisotropic contraction
Energy under
isotropic contraction
Free energy Efree , a.u.
Aspect ratio Ly/Lx
(a) εzz = 0.050
(b) εzz = 0.051
(c) εzz = 0.052
(d) εzz = 0.053
(e) εzz = 0.055

Fig. 7.

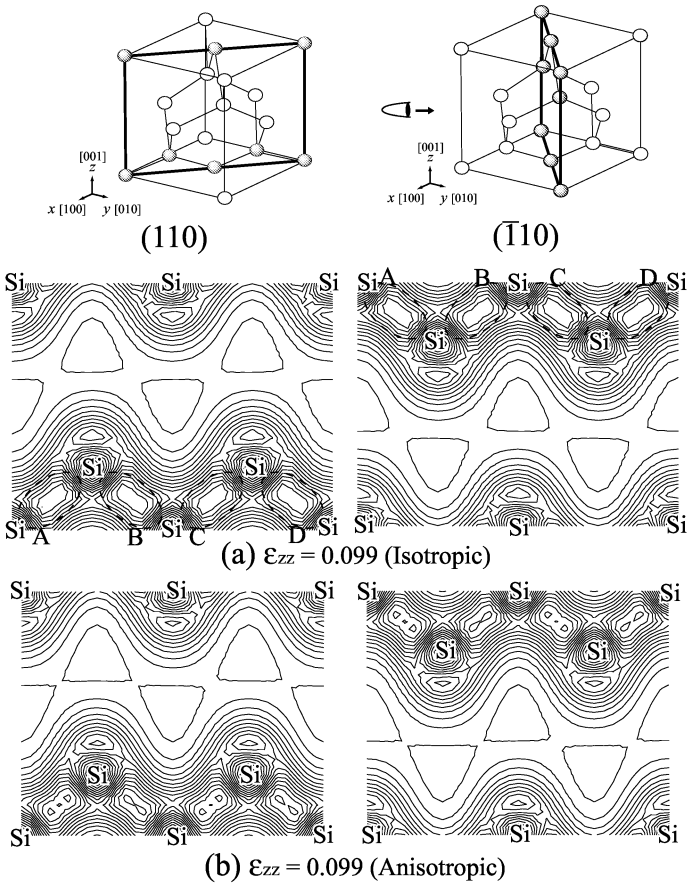
[001]
z
x [100]
y [010]
(110)
(1̄10)
Si
A
B
C
D
(a) εzz = 0.099 (Isotropic)
(b) εzz = 0.099 (Anisotropic)

Fig. 8.

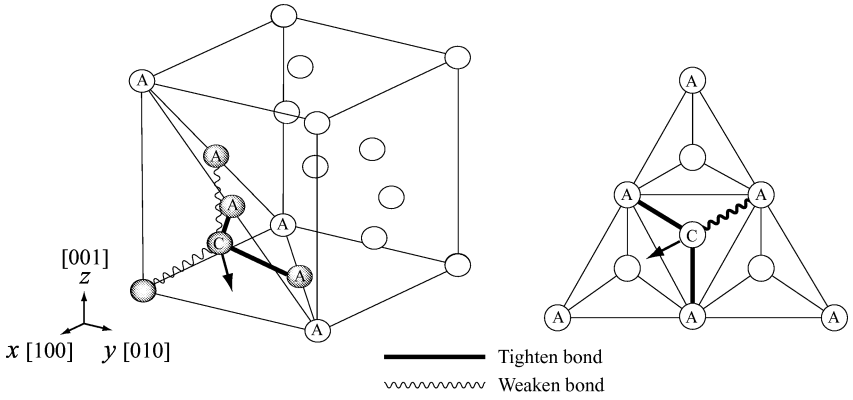
[001]
z
x [100]
y [010]
A
C
Tighten bond
Weaken bond

Fig. 9.

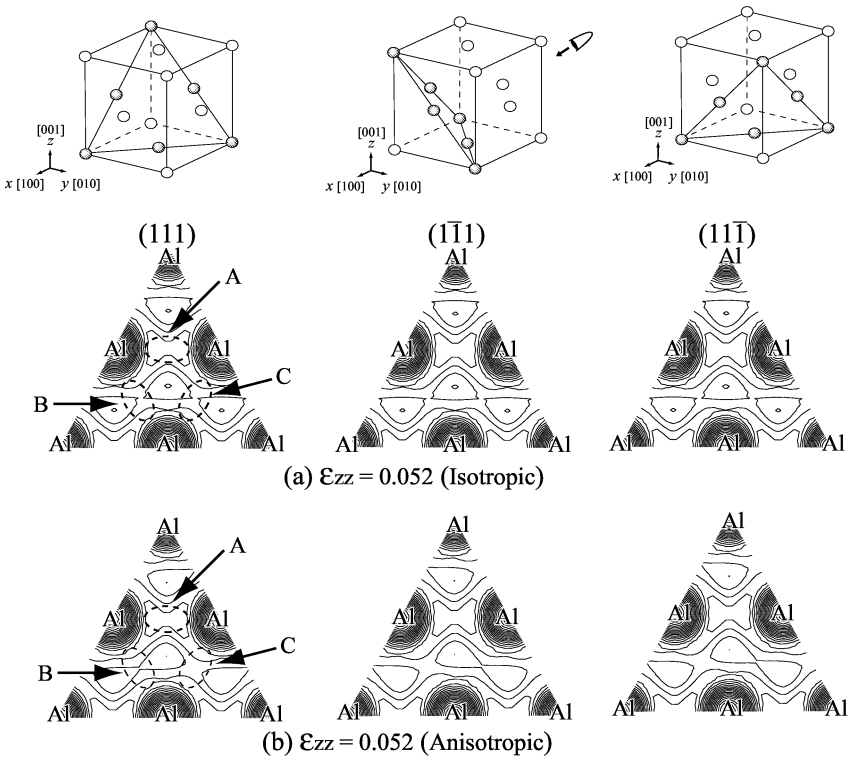
[001]
z
x [100]
y [010]
(111)
(1$\bar{1}$1)
(11$\bar{1}$)
Al
A
B
C
(a) Ezz = 0.052 (Isotropic)
(b) Ezz = 0.052 (Anisotropic)

Fig. 10.

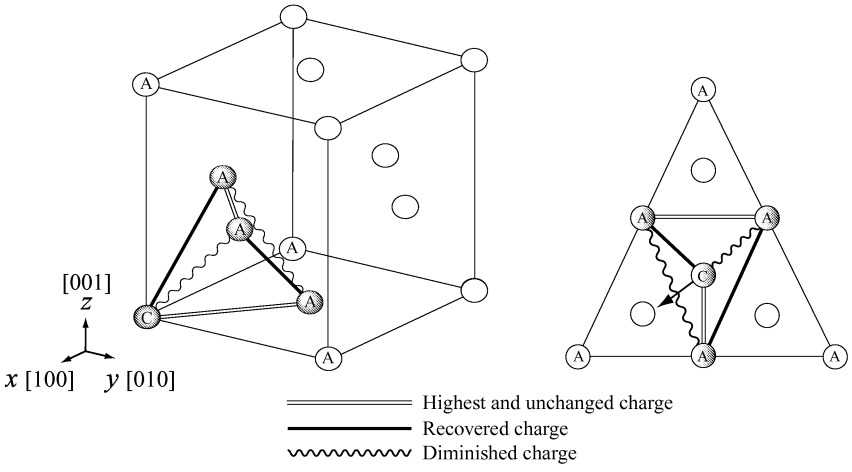
[001]
z
x [100]
y [010]
A
C
Highest and unchanged charge
Recovered charge
Diminished charge

Fig. 11.